JOURNAL OF COMPUTATIONAL PHYSICS **137,** 265–298 (1997)
ARTICLE NO. CP975768

A Riemann Problem Based Method for the Resolution of Compressible Multimaterial Flows

Jean-Pierre Cocchi and Richard Saurel

Institut Universitaire des Systèmes Thermiques Industriels, CNRS-UMR 6595, 5 rue Enrico Fermi, 13453 Marseille Cedex 13, France

Received January 17, 1996; revised May 13, 1996

A correction for Godunov-type methods is described, yielding a perfect capture of contact discontinuities, in hydrodynamic flow regime. The correction is based upon a simple idea: starting from a nondegraded solution at a given instant, the use of an Eulerian scheme around a contact discontinuity will entail, at the next instant, the degradation of the solution at only the two adjacent nodes to the discontinuity. The exact solution of the Riemann problem yields the state variables on both sides of the discontinuity. Knowledge of these variables may be used to correct the two nodes affected by numerical diffusion. The method is applied to problems involving a gas–liquid interface. The liquid is assumed compressible, obeying the ''stiffened gas'' equation of state, for which the solution of the Riemann problem is easily obtained. The method is first tested with 1D problems which have either an exact solution or accurate numerical solutions in the literature. Then the concept is extended in two dimensions. Assuming that the 1D Riemann problem along the normal to the interface is a reasonable approximation of the 2D Riemann problem for Euler equations, we extend efficiently the algorithm for two-dimensional interface problems. Several two-dimensional test cases are presented for which the method provides accurate solutions.

© 1997 Academic Press

1. INTRODUCTION

Most numerical methods applied to the Euler equations, are affected by numerical diffusion, due to truncation errors. This entails a smearing of the shock waves and contact discontinuities. Among the methods that allow the computation of shock

0021-9991/97 $25.00
Copyright © 1997 by Academic Press
All rights of reproduction in any form reserved.

waves and contact surfaces or, more generally, discontinuities in gas dynamics, two main categories may be distinguished:

—Shock-capturing methods which are the most commonly used;

—Front-tracking methods.

Shock capturing methods are essentially Eulerian schemes and have been considerably improved in the last 20 years, involving Riemann problem based methods, or high-order extensions of Godunov's [14] scheme. One may cite, among these, the schemes due to Van Leer [32], Roe [27], Osher [25], Collela and Glaz [5], as well as others, like the flux corrected transport algorithm FCT (Book *et al.* [3]), not based on the Riemann problem.

The second category involves generally a combination of Euler and Lagrange schemes, the latter providing the treatment of contact discontinuities. One may cite the papers of Chern *et al.* [4], and the more recent ones of De Kang Mao [8–10]. Mulder *et al.* [24] have developed a Hamilton–Jacobi formulation for the motion of interfaces to simulate Rayleigh–Taylor and Kelvin–Helmholtz instabilities.

Shock-capturing methods, although considerably improved, always yield a numerical diffusion of discontinuities, over several nodes. These shock-capturing algorithms are based upon two concepts: the earlier one is that of artificial viscosity, while a more recent one is that of flux limiters. The first concept, due to Von Neumann and Richtmyer [33], adds a dissipative term to the equations, thus spreading the discontinuity over a finite-thickness zone. Flux limiters reduce high order schemes to first order at discontinuities, providing stable solutions. This yields a finer capture of the discontinuities, but still with a finite thickness.

Numerical diffusion, however small, is nevertheless unacceptable in certain circumstances. It is the main motivation of the present study. Consider, for example, an interface separating two gases of differing specific heat ratios: Abgrall [1] and, later, Karni [20] have shown that classical shock-capturing methods fail in this case. Another example, even more significant and at the basis of the present work, is that of an interface separating a gas (governed by its own equation of state) from a liquid, or a compressible solid, governed by another equation of state. When numerical diffusion appears the density diffuses from one medium to the other, producing a nonphysical zone, in which the computation of the pressure obtained by any of these two equations of state is without sense: the equations of state are not continuous across the interface.

To remedy this defect, one must achieve a zero-point interface capturing. Many researchers have developed specific techniques for accurate resolution of shocks and interfaces in order to minimize numerical diffusion when conservation equations are solved. However, to the exception of the ''random choice method'' (Chorin [7], Glimm [16]), which yields a really fine resolution of shocks and contact surfaces, the resolution offered by other methods, such as Osher's ENO scheme [25], is at best of 2 to 3 nodes. On the other hand, despite its superiority in shock capturing, the ''random choice method'' is subject to some drawbacks; due to the randomness of the method, the computed positions of the various waves are correct on average only, while expansion waves contain oscillations. Furthermore, that algorithm fails in

two dimensions. Regarding the other techniques, the improvement of the resolution often involves the use of a higher-order scheme.

The object of the present study is to simulate fluid-dynamic problems, involving interfaces separating different materials. The behavior of each material being described by its own equation of state, numerical diffusion is forbidden, since it prohibits the use of the equation of state. So, Eulerian methods are ill-adapted.

By opposition to Eulerian methods, the Lagrangian approach seems to be more convenient for the interface capturing. Lagrangian methods are characterized by the fact that the mesh moves with material particles. Thus, the mesh nodes coincide always with the same particles, in particular with those of the contact surfaces. It should be pointed out, however, that the presence of strong velocity gradients may lead to geometrical singularities of the mesh grid, due to excessive distortions of its elements, and may produce a degradation of the solution. In addition, fluid-dynamic problems almost always involve fluid inflows and outflows, which correspond to adding and/or subtracting mesh nodes. Therefore, Lagrangian methods are ill-adapted to general fluid-dynamic problems.

The drawbacks of both Eulerian and Lagrangian methods have led us to develop a strategy including the advantages of each method, but with minimum inconveniences. The proposed method involves a standard Eulerian predictor step, followed by a corrector step applied only to nodes adjacent to the interface. The latter step is, in a certain way Lagrangian, however, without using a specific Lagrangian scheme. The corrector step consists in interpolating the values at nodes on both sides of the interface, using the values at neighbouring nodes, which have not suffered of numerical diffusion, and the values obtained by the resolution of the Riemann problems at the interface. The overall scheme is very simple in one space dimension and no more expensive in computer time than the Eulerian scheme. The Eulerian scheme avoids mesh distortion and allows the determination of all fluid variables at each node of the discretized domain, except for nodes that are situated on both sides of the interface. The latter are subsequently corrected by linear interpolation. Since the resolution is performed on a fixed grid, the time step is from the Eulerian scheme and does not suffer of mesh size reduction like for Lagrangian schemes.

The proposed front tracking method produces an excellent interface handling, both for its location and for the description of its geometry. So, the method is perfectly suited to maintain fine resolution of contact discontinuities. However, new contact discontinuities may appear during the flow evolution. The proposed technique cannot unfortunately treat them if they are not created in perfectly known locations in the flow. This is a limitation of the method.

For problems involving gases of different natures the solution of the Riemann problem, upon which the present strategy is based, poses no particular problem. For flowfields in which a liquid–gas interface is present, the liquid will always be considered as compressible; the solution of the Riemann problem is rendered easy by the choice of a convenient equation of state: the ''stiffened gas'' equation of state. At the liquid–gas interface, it suffices to carry out the correction step by solving a mixed Riemann problem, i.e. with different equations of state on each side.

This front tracking technique is first tested and validated on several one-dimensional test cases. It is then extended to two dimensions. This extension is realized

by the operator splitting technique for the Eulerian predictor step. Because of geometrical and physical difficulties, the two-dimensional treatment is more complicated than it is in one dimension. The interface is materialized in two dimensions by a chain of markers connected by line segments. The determination of marker velocity and states on both sides of the interface is obtained by the resolution of the exact Riemann problem along the normal to the interface. To propagate the front it suffices, thus, to move each marker with the local velocity. Corrections of nodes affected by numerical diffusion are performed by extending the ideas developed in one dimension. Nevertheless, some care must be taken since the interface may have a singular topology for which specific treatments are necessary. They will be presented in detail.

The proposed method is then applied to the computation of a two-dimensional flowfield that includes a liquid–gas interface, a gas–gas interface, and others. One presents some calculations which show the capabilities and the accuracy of the method on four test cases. The first concerns the motion of a gas bubble in a liquid. The second and third concern a simplified model of underwater explosion. Finally, the last one is the interaction of shock wave with a gas bubble.

2. BASIC IDEAS IN ONE-DIMENSION

2.1. Analysis

In the present work, one seeks to develop a method that could be applied to problems involving interfaces which separate fluids with different properties, but under circumstances such that viscous or heat-flux effects are negligible by comparison with pressure-related effects. Then, the governing equations are the well-known Euler equations,

$$\frac{\partial U}{\partial t} + \frac{\partial F(U)}{\partial x} = 0, \tag{1}$$

with

$$U = \begin{bmatrix} \rho \\ \rho u \\ e \end{bmatrix} \qquad F(U) = \begin{bmatrix} \rho u \\ \rho u^2 + p \\ u(e + p) \end{bmatrix}, \tag{2}$$

where ρ is the density, u is the velocity, p is the pressure, and e is the total energy per unit volume.

The stiffened gas equation of state. The stiffened gas equation of state employed here is detailed in Harlow and Amsden [17], Plohr [26], Menikoff and Plohr [23],

$$E = \frac{1}{N-1}\frac{(p + Np_\infty)}{\rho}, \tag{3}$$

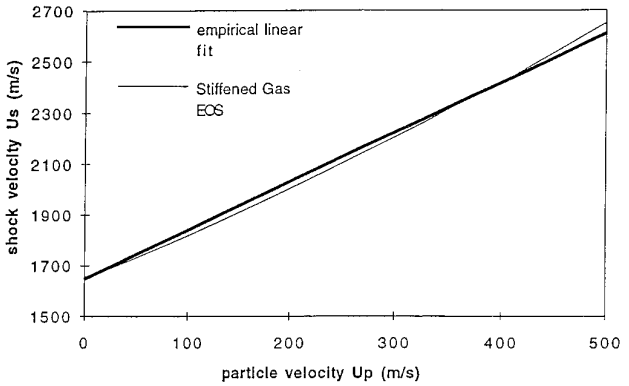

FIG. 1. Experimental and computed Hugoniot curves.

where $E = e/\rho - \frac{1}{2}u^2$ is the internal energy, N and p_∞ are parameters characteristic for each material (liquid, gas, and solid).

Determination of the parameters N and p_∞. As it mentioned in Plohr [26], the experimental Hugoniot curve of a material links the shock velocity, $U_s = |\omega - u_0|$ to the particle velocity $U_p = |u - u_0|$. These experimental data show that the relationship between U_s and U_p may be reasonably approximated by a linear function

$$U_s = a_0 + \alpha U_p, \tag{4}$$

where a_0 is the sound velocity of material at rest and α is a dimensionless constant. For water, $a_0 = 1647$ m/s, $\alpha = 1.921$.

Then, using Hugoniot relations and the stiffened gas equation of state, one deduces a relationship between U_s and U_p which is

$$U_s = \left[a_0^2 + \left(\frac{N+1}{4} U_p \right)^2 \right]^{1/2} + \frac{N+1}{4} U_p. \tag{5}$$

As illustrated in Fig. 1, within an interval of material velocity variations, one may determine the value of N giving the closest agreement between the empirical linear fit of the experimental data and Eq. (4).

Once the coefficient N is known, the value of p_∞ is determined by

$$p_\infty = \frac{\rho_0 a_0^2}{N} - p_0. \tag{6}$$

For water, the results are: $p_\infty = 4921.15$ bars, $N = 5.5$.

For a gas, the above procedure is not necessary. Identification with the ideal gas equation of state, yields to $p_\infty = 0$ and $N = \gamma = 1.4$ (for example).

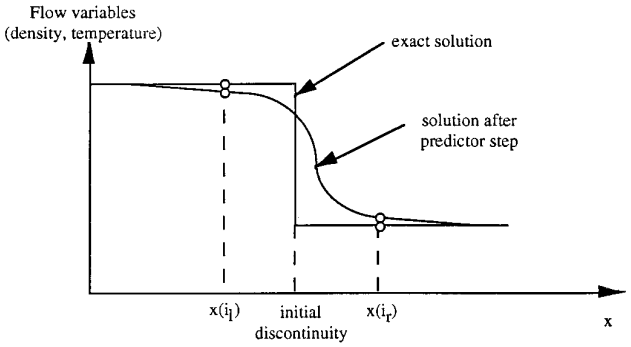

FIG. 2. Diffusion of the contact discontinuity.

2.2. Predictor Step

The numerical algorithm begins with a predictor step which is followed by a corrector step. The predictor step may use any Eulerian scheme. However, since the correction step will employ the solution of the Riemann problem (RP), it is logical to use a Riemann problem based method for the predictor step. The Eulerian scheme that is used may be a first or higher order scheme. The choice of the method order depends on the accuracy required by the user for nodes away from the interface. If a high accuracy in the shock capture is not required, Godunov's scheme will suffice; it will be now briefly recalled.

Godunov's scheme. Godunov [14] proposes a first-order accurate scheme in time and space which may be written as

$$U_i^{n+1} = U_i^n - \frac{\Delta t}{\Delta x}[F(U_{i+1/2}^{*n}) - F(U_{i-1/2}^{*n})], \tag{7}$$

where $F(U_{i\pm1/2}^{*n})$ are determined from the solution of the Riemann problem across the surface situated at the abscissa $x_{i\pm1/2}$.

If higher accuracy is required in the capture of shock and rarefaction waves, Godunov's scheme may be extended to second order by using the basic concepts of Van Leer [32] (see also Toro [31] for an overall description of second-order schemes).

2.3. Correction Step

Starting from a perfectly localized discontinuity, at a given instant (the initial instant, for example) the problem consists in determining its position at next instants and the values of the flow variables on both sides of the discontinuity. The basic idea of the method is that the Eulerian scheme being applied at the predictor step, as described above, will generate a numerical diffusion over two nodes only, during a single time step. Nodes affected by numerical diffusion that are situated on the left (i_l) and on the right (i_r) of the interface are represented in Fig. 2.

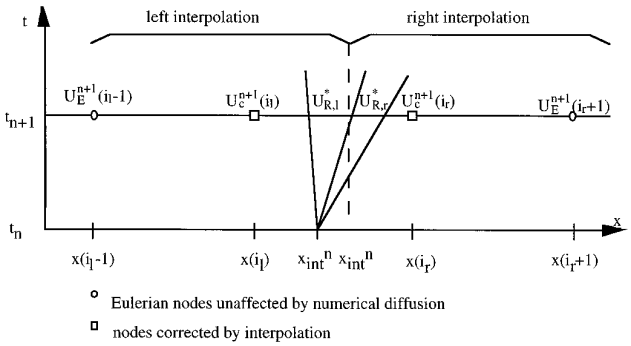

FIG. 3. Interpolation of points surrounding the interface.

Now, if we correct the two erroneous nodes, a perfect discontinuity will be recovered, thus allowing the computation of the next time step. The correction is carried out by a simple interpolation between the state variables given by the solution of the Riemann problem and those of the neighboring nodes not affected by numerical diffusion.

Resolution of the exact Riemann problem at the interface, with the statevectors U_{il}^n (at the left) and U_{ir}^n (at the right), allows the computation of the interface velocity u^*, as well as the flow variables at the left and right sides of the interface, at instant t_{n+1}. Now, having determined the interface velocity u^* and its spatial location, the interface is moved between t_n and t_{n+1}. The movement of the interface is given by

$$\frac{dx_{\text{int}}}{dt} = u^*, \tag{8}$$

where the velocity u^* is assumed constant over a time step.

When correction of the diffused nodes is carried out on both sides of the interface, at instant t_{n+1}, two instances may occur: the first corresponds to the case where the interface stays within the same cell; the second occurs when the interface crosses from one cell to another between instants t_n and t_{n+1}. In the first occurrence, the flow variables at nodes i_l and i_r are determined at instant t_{n+1} by linear interpolations on both sides of the interface, as shown in Fig. 3. The statevector $U_c^{n+1}(i_l)$ at the node of abscissa $x(i_l)$ is computed from the states $U_E(i_l - 1)$ and $U^*_{R,l}$ by linear interpolation:

$$U_c^{n+1}(i_l) = \frac{x(i_l) - x(i_l - 1)}{x_{\text{int}}^{n+1} - x(i_l - 1)} (U^*_{R,l} - U_E^{n+1}(i_l - 1)) + U_E^{n+1}(i_l - 1). \tag{9}$$

U_E denotes the state which is obtained by the Eulerian scheme, whereas U_R denotes the solution of the Riemann problem, computed from the left-side (i_l) and right-side (i_r) variables at instant t_n.

Flow variables at node of abscissa $x(i_r)$, are obtained similarly.

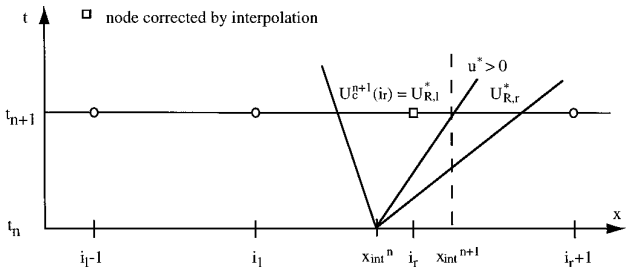

FIG. 4. Case where the interface leaves the cell.

The second case corresponds to the situation where the interface leaves the cell between instants t_n and t_{n+1}. The distinction from the previous case is that the nodes i_l and i_r are on the same side of the interface. In such a situation, two instances must be envisaged:

1. if $x_{\text{int}}^{n+1} > x(i_r)$, then $U_c^{n+1}(i_r) = U^*_{R,l}$, $p_\infty(i_r) = p_{\infty,l}$ and $N(i_r) = N_l$ (10)
2. if $x_{\text{int}}^{n+1} < x(i_l)$, then $U_c^{n+1}(i_l) = U^*_{R,r}$, $p_\infty(i_l) = p_{\infty,r}$ and $N(i_l) = N_r$. (11)

Figure 4 illustrates, as an example, the first case.

The capabilities of this simple method are now illustrated on three one-dimensional test cases.

2.4. Validation of the Proposed Method

A shock tube with two different gases. The test case originally proposed by Abgrall [1] and investigated by Karni [20] and Abgrall [2], is considered. It concerns a shock tube containing two different gases having different specific heat ratios. Karni emphasizes the encountered difficulties and discusses means to remedy them. She proposes to solve the system of Eqs. (1) in its primitive form, in order to treat correctly the interfaces. However, some troubles appear when the shock wave interacts with the interfaces. In our approach, the Euler equations are solved in conservative form, while the interface is treated as discussed above. Consider a shock tube of 1-m length, including two chambers, separated by a fictitious diaphragm at the 0.5-m abscissa. Initial conditions for the problem are:

$$x < 0.5, \quad \rho_l = 0.192, \quad u_l = 0.0, \quad p_l = 1.2 \text{ bar}, \gamma_l = 1.6667;$$
$$x \geq 0.5, \quad \rho_r = 1.156, \quad u_r = 0.0, \quad p_r = 1.0 \text{ bar}, \gamma_r = 1.4.$$

The results presented in Figs. 5 and 6 have been obtained either by a second-order Eulerian scheme, designated "results without correction," or by the new scheme designated "results with correction." As discussed above, the computation without correction takes into account for change of γ across the interface, by using a species conservation equation as is usually made for reactive flows. The computation with correction uses two different specific heat ratios, γ_l and γ_r, characteristic of each medium. The exact solution is also represented.

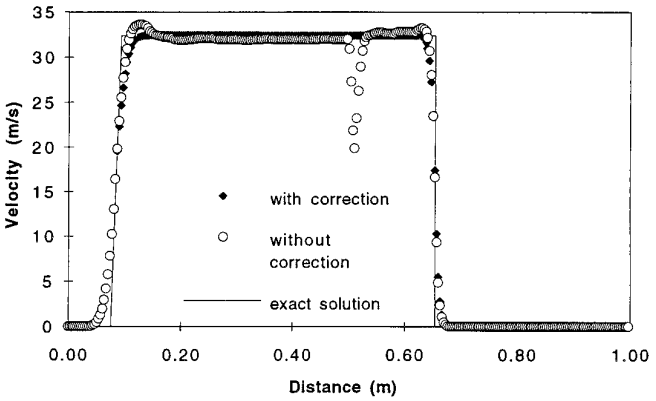

FIG. 5. Velocity distribution.

Results corresponding to the instant $t = 15$ μs after the diaphragm rupture are shown in Figs. 5 and 6. Figure 5 gives the evolution of the velocity along the shock tube. For the computation without correction, one may notice a nonphysical oscillation across the interface. This oscillation disturbs the resolution of the flow-field and generates further oscillations at the shock and at the expansion tail. The computation with correction removes all oscillations and, in addition, produces a perfect matching of the velocities across the interface. Figure 6 represents the density evolution. The interface given by the computation without correction is slightly diffused, whereas it is perfectly captured with the new method. Figures 5 and 6 show that the new algorithm is efficient on this test case, while the classical procedure used for reactive flows fails.

A two-phase gas–liquid shock tube. The test case of a particular shock tube, shown in Fig. 7, is now investigated; the tube contains in its left-side compartment a high-pressure gas, while on the right side it is filled with liquid at atmospheric pressure. This test case is of interest since it allows us to test the method on a

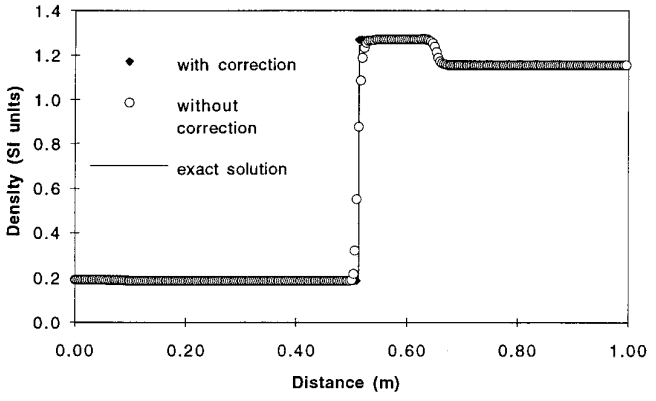

FIG. 6. Density distribution.

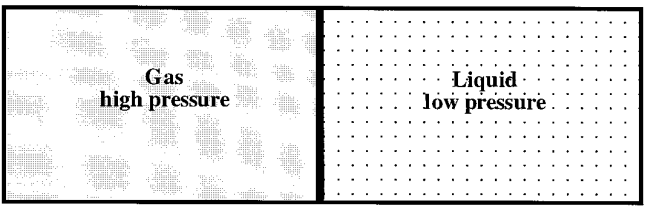

FIG. 7. Initial configuration of the shock tube.

problem involving two fluids governed by two different equations of state. Moreover, an exact solution for this test case is available.

The solution is carried out with the first-order predictor step and then with the second-order one. Figures 8 and 9 show that the second-order method provides a better capturing of the shock wave as anticipated. Figure 9 shows that the first-order computation generates some errors at the interface, since the curve marked with diamonds is slightly curved on both sides of the interface. The second-order scheme corrects this small defect well. The positions of the shock, the interface, and the expansion wave, as well as the magnitudes, of the various variables related to the shocked liquid and to the expanded gas are analytically verified. One may state that the new method works correctly in a case involving the presence of two fluids governed by different equations of state. The results obtained by a strictly Eulerian scheme are not presented here because the calculations fail at the second time step.

Underwater explosion. Now the new method is applied to the problem of an underwater explosion previously investigated by Flores and Holt [12] and Cooke and Chen [6]. The new method distinguishes itself from the former one by the use of a Riemann problem especially suited to a stiffened gas equation of state and, also, by a specific treatment of the liquid–gas interface. Flores and Holt used the ''random choice'' method, while Cooke and Chen employed the technique of

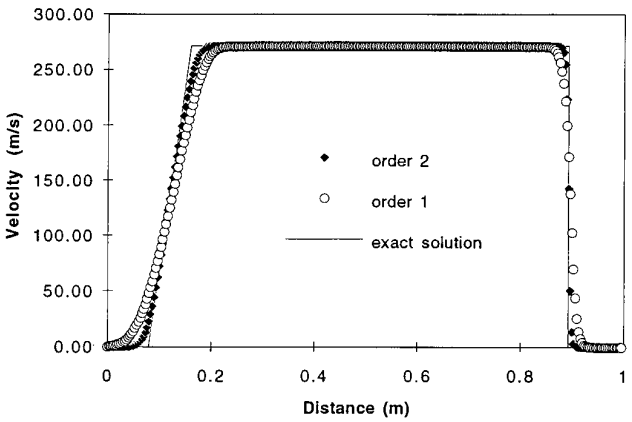

FIG. 8. Velocity distribution.

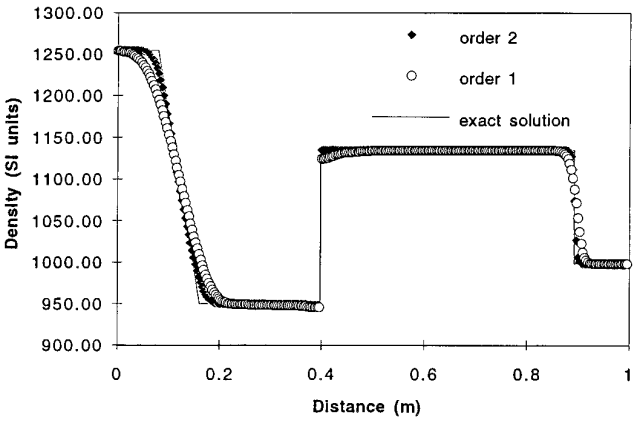

FIG. 9. Density distribution.

"continuous front tracking with subcell resolution." Their results will be compared to ours, thus validating the present approach.

The underwater explosion problem involves a spherical wave pattern. In order to be able to treat exactly such a problem, a "spherical" Riemann solver should be necessary. Construction of such a solver is not easy at all. Here the technique of operator splitting is adopted, which consists in using the solution of the Riemann problem for the plane geometry and taking into account for the spherical terms as source terms. Within the framework of the algorithm described above, it suffices to supplement it with an integration step for the differential system

$$\frac{dU}{dt} = H(U, r) \quad \text{with } H(U, r) = -2 \begin{bmatrix} \dfrac{\rho u}{r} \\ \dfrac{\rho u^2}{r} \\ \dfrac{u(e+p)}{r} \end{bmatrix}, \tag{12}$$

where U is the solution obtained after the correction step of the preceding algorithm.

Our simplified model of underwater explosion does not take into account for the ignition and propagation of the detonation and, moreover, assumes that the reaction products obey the ideal gas law.

In the configuration investigated here, the gas is initially confined, at high pressure $p_{0,g}$ and temperature T_0, within a sphere of radius R_0. The problem may be reduced to that of a shock tube problem with a spherical diaphragm that separates the high-pressure gas from a liquid at atmospheric pressure. Using the new method, one should verify that the liquid–gas interface is correctly captured and followed in time, in such a spherical geometry. The initial conditions are summarized in Table I.

Here, all variables are rendered nondimensional, as in [6], in order to have comparable results. Lengths are referred to the characteristic length h(depth).

TABLE I
Initial Data

Charge radius, R_0	1/3 ft
Depth of charge at center, h	1 ft
Initial pressure of detonation products	9000 atm
Initial temperature of detonation products	2500 K
Initial liquid pressure	1 atm
Stiffened Gas EOS parameters for the gas	$N_1 = 1.4$, $p_{\infty,1} = 0$
Stiffened Gas EOS parameters for the liquid	$N_2 = 5.5$, $p_{\infty,2} = 4921.154$

Velocities are divided by the sound velocity in the unshocked liquid and computed by Tait's equation of state, as u/a_0. Densities are given as $\rho/\rho_0(\rho_0 = 1007\ \text{kg/m}^3)$. Pressures are referred as $p/(p_0 + B)$, where B is one of the constants in Tait's equation. The space step is chosen as $\Delta r = 0.0001$ (300 cells over a length of 1 ft).

Contrary to other authors, instead of Tait's equation of state, the stiffened gas equation is adopted, since its coefficients are readily calculated from the experimental Hugoniot curve as discussed above. The stiffened gas EOS allows an easy treatment of different materials; whereas Tait's equation of state is not easily adaptable to other materials and is mainly employed for shocked water.

Figures 10 and 11 correspond to the instant $t = 4.55\ \mu$s after the diaphragm rupture. Our curves, obtained by a second-order computation, fit exactly with those of the cited authors, for the gas side. Some slight differences are present on the liquid side, due to the fact that Cooke and Chen [6] use Tait EOS, while we use the stiffened gas EOS.

Figure 10 gives the radial velocity evolution. One may notice that the velocity is higher near the expansion wave than behind the shock. Actually, as the shock travels away from the charge center, its strength decreases, while the intensity of the expansion wave increases when it propagates to the center. The positions of the shock and of the expansion wave, as well as the overall curve shape, are in

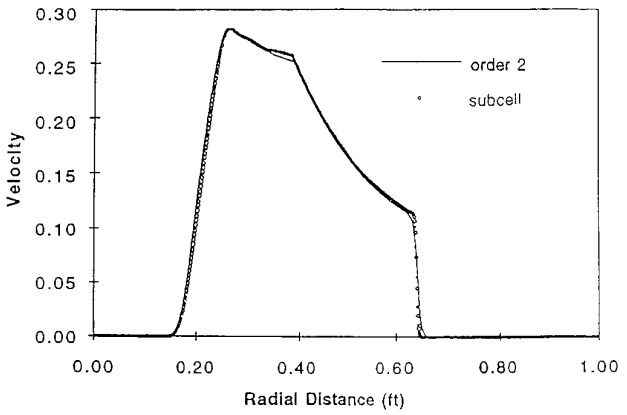

FIG. 10. Velocity distribution.

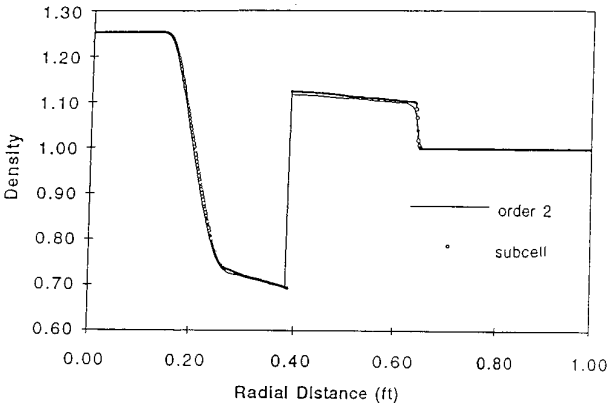

FIG. 11. Density distribution.

good agreement with those of Cooke and Chen. On the other hand, and despite the use of a second-order algorithm, their shock capturing is better than ours because of the use of the ENO scheme (Harten [18]). Better shock capturing could be performed by our method using, for example, the Superbee flux limiter (Roe [27]) at the predictor step. However, our main goal is to elaborate a numerical method for interfaces.

The density distribution is shown in Fig. 11. As pointed out above, the shock strength falls while it travels into the liquid medium. For this reason, we have a slight decrease in density in the shocked liquid region. The slight difference between our density curve of the shocked liquid and that of Cooke and Chen [6] is due again to the different equations of state used. Excepting this difference, the quality of the results is quite satisfactory.

Comparison between our results and those of Cooke and Chen [6] shows that the new method produces results as good as those of "continuous front tracking with subcell resolution."

3. TREATMENT OF A TWO-DIMENSIONAL INTERFACE

In this part, we describe the treatment of an isolated interface in two dimensions. We are going to extend the front tracking and the correction step given in the one dimensional case in two dimensions. Resolution of Euler equations during the predictor step is easily adaptable in two dimensions by using alternative direction splitting. However, the front tracking and corrections associated with it are more difficult. Contrarily to the one-dimensional case, it is necessary to use two correction steps which will be detailed below. Furthermore, the interface can take particular positions in the mesh and it is necessary to elaborate specific corrections. In the following subsections, we shall show these difficulties and describe how to overcome them.

3.1. Eulerian Predictor Step

Alternative direction splitting. One adopts here the alternative direction splitting, that allows to employ the previously presented algorithm, alternatively to the two

spatial directions. The fact that an alternative direction splitting on a regular mesh is used, does not constitute a very important restriction of the present method. Indeed, the principle of alternative direction splitting does not produce specific errors, compared to the two-dimensional classical methods.

Two-dimensional Euler equations may be written in conservative form,

$$\frac{\partial U}{\partial t} + \frac{\partial F(U)}{\partial x} + \frac{\partial G(U)}{\partial y} = 0 \tag{13}$$

with

$$U = [\rho, \rho u, \rho v, e]^{\mathrm{T}}, \quad F(U) = [\rho u, \rho u^2 + p, \rho uv, (e + p)u]^{\mathrm{T}},$$
$$G(U) = [\rho v, \rho uv, \rho v^2 + p, (e + p)v]^{\mathrm{T}},$$

where (u, v) are coordinates of the velocity vector and e is the total energy per unit of volume defined by

$$e = \frac{p + Np_\infty}{N - 1} + \frac{1}{2}\rho(u^2 + v^2). \tag{14}$$

The alternative direction splitting replaces the system of two-dimensional Euler equations in two sets of one-dimensional equations. Solution is now obtained by a succession of one-dimensional operator (Strang [29]).

$$U_i^{n+1} = L_x^{\Delta t/2} L_y^{\Delta t} L_x^{\Delta t/2} U_i^n. \tag{15}$$

Each one-dimensional operator (x step example) consists in the resolution of the one-dimensional system (1), augmented by Eq. (16) for the tangential velocity component determination,

$$\frac{\partial \rho v}{\partial t} + \frac{\partial \rho uv}{\partial x} = 0. \tag{16}$$

Equation (16) may be transformed into

$$\frac{\partial v}{\partial t} + u\frac{\partial v}{\partial x} = 0. \tag{17}$$

This last equation shows that the tangential velocity component is a Riemann invariant along the u direction. So it is easy to complete the 1D Riemann solver for the splitted 2D equations.

3.2. Correction Step

3.2.1. *Front Tracking*

To implement the correction step, it is first necessary to know initially the interface position that must be tracked during resolution. The proposed method is a marker-

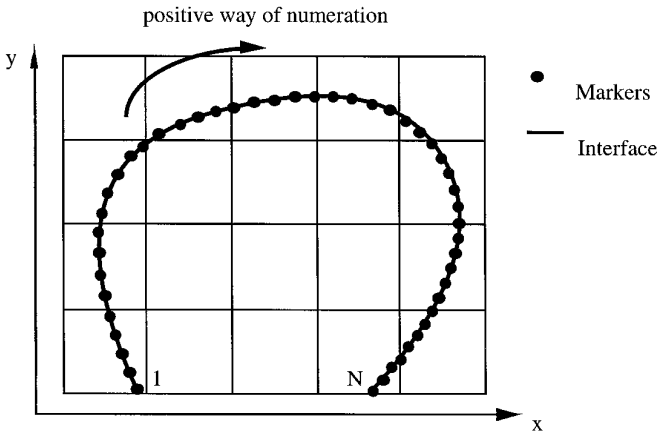

FIG. 12. Interface approximated by a succession of markers.

and-cell type tracking method [17]. The discussion on the distribution of markers on the interface to the computed solutions has been considered previously by Gardner *et al.* [13]. This distribution is illustrated in Fig. 12.

Determination of states on both sides of the interface. The interface is represented by a succession of line segments, connected between them with markers. These markers are mainly useful for the building and the motion of the interface. When the interface is perfectly defined and localized spatially at instant t_n, it is necessary to determine states on both sides of the contact discontinuity in order to activate nodes of the mesh in liquid or in gas and to realize the necessary corrections.

In all rigor, the propagation of the interface and the correction of Eulerian nodes on both sides of the interface, in the two-dimensional case, would need a two-dimensional exact Riemann solver. During these last years, multidimensional extensions of the linear Roe solver have been made. According to authors, it does not currently exist any two-dimensional exact Riemann solver. Since this tool is not available, one uses the solution of the one-dimensional exact Riemann problem, at the points of intersection between the mesh and the interface, following the normal to the interface, as done by Leveque and Shyue [22] for shock tracking. Solution of the one-dimensional Riemann problem along the normal to the interface is an approximation of the two-dimensional Riemann problem. In many cases, this approximation is acceptable, as one will see in examination of the results. But there exist two-dimensional configurations for which the actual algorithm fails. These specific configurations will be shown thereafter.

Resolution of the Riemann problem along the normal at the interface. First, we determine points of intersection between line segments and mesh lines at instant t_n. To localize each point of intersection in the mesh we define around each node, a rectangular area of Δx length and Δy width, as defined in Fig. 13. We then determine to what area the considered point of intersection belongs. This defines the horizontal line i or the vertical line j of the mesh on which states at points

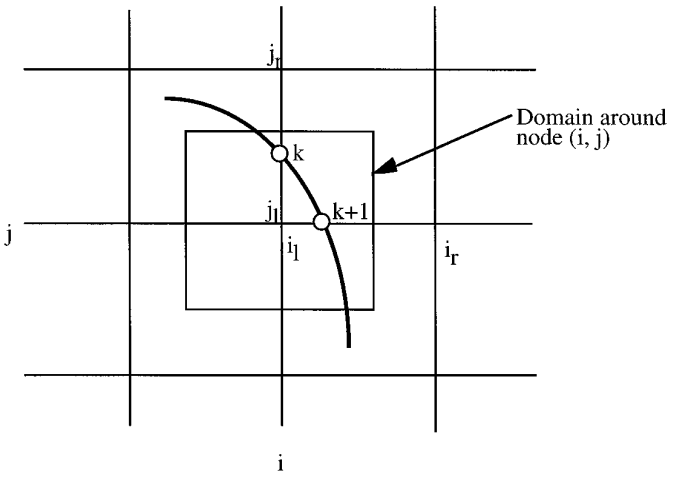

FIG. 13. Location of points of intersection in the mesh.

indexed by i_l, j_l, i_r, and j_l, will be used for the resolution of the Riemann problem (see Fig. 13).

Similarly to the one-dimensional case, we seek indexes of Eulerian nodes surrounding the interface. When the interface cuts a horizontal line of the mesh, one can determine indexes of neighboring nodes, i_r and i_l. A couple of statevectors (U_l, U_r) is associated to these indexes. The exact Riemann problem is solved from these statevectors. In the one-dimensional case, determination of states l* and r* is trivial, since the resolution of the Riemann problem is achieved only by following the x-direction. However, it is more complicated in the two-dimensional case. Indeed, the two-dimensional resolution is no longer valid in the x or y direction, but by following the normal to the interface. Due to the fact that statevectors U_l and U_r are situated on mesh lines and that resolution of the Riemann problem is realized by following the normal to the interface, it is therefore necessary to realize the projection of these statevectors along the normal.

As shown in Fig. 14, a local frame of reference (k, $\vec{T}$, $\vec{N}$) is defined at the point of intersection k. $\vec{N}$ and $\vec{T}$ are the normal and tangential vectors to the interface at point k.

The orientation of normal vector $\vec{N}$, allows us to identify media on both sides of the interface. This information is capital for the activation process of Eulerian nodes in a gas or liquid and the correction of nodes altered by numerical diffusion.

In Fig. 14, right and left statevectors, following the normal vector $\vec{N}$ to the interface, are noted $U_{n,r}$ and $U_{n,l}$. These statevectors are obtained by projection of the states U_r and U_l in the new local frame of reference.

Resolution of the Riemann problem. From statevectors $U_{n,r}$ and $U_{n,l}$ the exact Riemann problem is solved and determines the statevectors $l^{*\prime}$ and $r^{*\prime}$, except for the tangential component of the interface velocity. As the interface moves in both directions, it is therefore necessary to determine the two velocities, u_n^* and v_t^* in the local frame of reference. It would be necessary, at this step, to use a two-

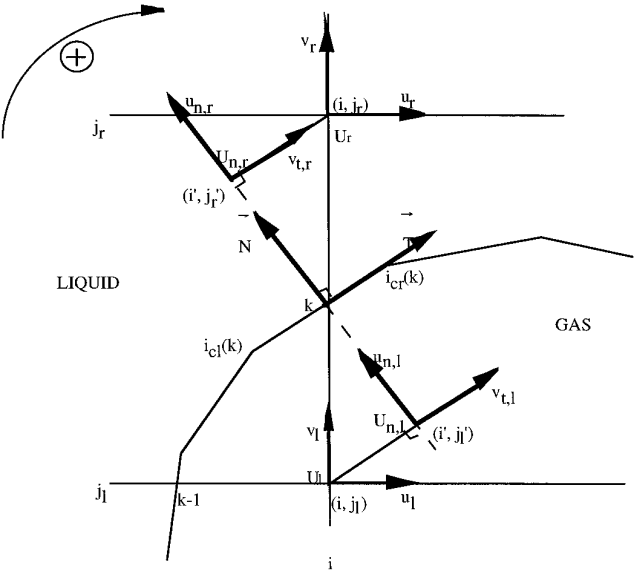

FIG. 14. Resolution of the Riemann problem following the normal.

dimensional exact Riemann solver. Absence of this solver is remedied by determining the tangential velocity component v_t^* from Eq. (17):

$$\begin{aligned} &\text{if } u_n^* \geq 0 \text{ then } v_t^* = v_{t,\mathrm{l}} \\ &v_t^* = v_{t,\mathrm{r}} \text{ otherwise.} \end{aligned} \tag{18}$$

The interface is an immaterial line which separates two compressible and different media having different tangential velocities. Since the flow is not dissipative, there may be some sliding between phases. As the tangential velocity is not determined accurately from the Riemann problem, we suppose that the tangential velocity of the interface at instant t_{n+1} is equal to the velocity of one of the two phases at instant t_n. The choice of the tangential velocity depends on the sign of the normal velocity u_n^*. We keep in mind that this approximation can have serious consequences in a strongly two-dimensional flow field.

After having determined in the local frame of reference all the hydrodynamic variables on both sides of the interface for all points of intersection, one returns to the main frame of reference $(0, x, y)$. Thus, velocities obtained by resolution of the Riemann problem and relationships (18) are all projected in this global frame of reference.

Now states on both sides of the interface are known for all points of intersection between the interface and the Eulerian mesh. We will next estimate these variables for all markers along the interface.

Determination of U_{R,l^*}, U_{R,r^*} for all markers. The purpose of this step is to determine the state variables on both sides of the interface along its contour.

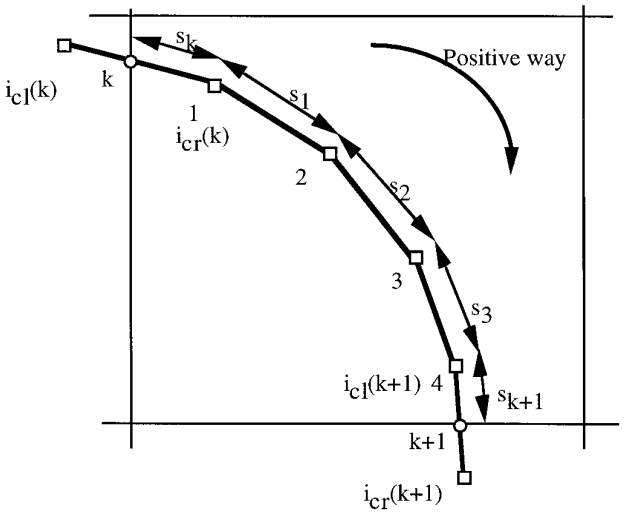

FIG. 15. Interpolation of variables for all markers.

Knowing U_{R,l^*}, U_{R,r^*}, u^*, and v^* for each point of intersection, we estimate these variables for all markers from linear interpolations, depending on the curvilinear abscissa. Consider two successive points of intersection k and $k + 1$. During the creation of the point of intersection k, we have memorized neighbor markers situated on both sides of the point k, indexed with $i_{cl}(k)$ and $i_{cr}(k)$ and, similarly, for the point $k + 1$. Knowing these indexes, we know exactly the number of markers situated between these two consecutive points of intersection as illustrated in Fig. 15.

For each marker we determine the length of the interface between the considered marker and the point of intersection k. This length expresses: $l_i = s_k + \sum_1^{i-1} s_j$, where s_k is the distance between the point of intersection k and the first marker following in the positive direction.

Identically, we estimate the total length $l_{\text{total}} = s_k + \sum_1^{Ne-1} s_j + s_{k+1}$ between the two points of intersection k and $k + 1$.

Components of the velocities and conservative variables for each marker are determined by linear interpolations,

$$\varphi(i) = \frac{l_i}{l_{\text{total}}}[\varphi(k+1) - \varphi(k)] + \varphi(k),$$

where $\varphi = U^*_{R,l}, U^*_{R,r}$. One can therefore calculate the propagation of the front for all markers of the interface with the next relationship,

$$\frac{d\overrightarrow{\text{OM}}_i}{dt} = \vec{\text{V}}^*_i, \tag{19}$$

where $\overrightarrow{\text{OM}}_i$ and $\vec{\text{V}}^*_i(u^*, v^*)$ represent the position and velocity of marker i.

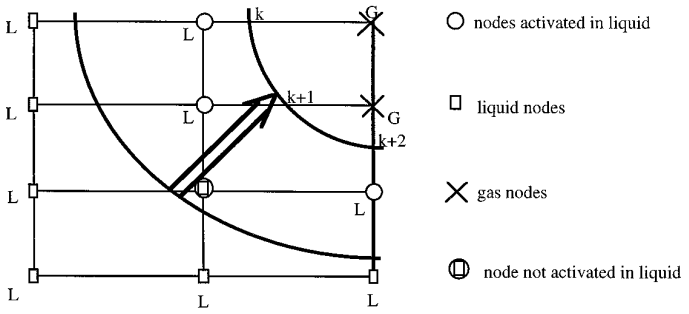

FIG. 16. Activation process of Eulerian nodes in liquid.

This new position of the interface is obtained at instant t_{n+1}, assuming no velocity variation during a time step. Points of intersection defined at instant t_n are also moved, since they will be used for the first correction step.

3.2.2. *Correction Step*

After having applied the Eulerian predictor step in the x or y direction, all Eulerian nodes surrounding the interface are altered by numerical diffusion and must consequently be corrected. The correction step consists thus, on the one hand, to correct erroneous points and, on the other hand, to activate Eulerian nodes in gas or in liquid if they are swept over by the interface. By opposition to the one-dimensional case, we use two correction steps in two dimensions. The first correction step consists of using projection of the old points of intersection defined at instant t_n and, second, to employ new points of intersection at instant $t_{n+1/2}$.

Here we detail the procedure for the first step of the alternative direction method. So the initial time is t_n and the final time is $t_{n+1/2}$. Corrections for the other sweep of the alternative direction method are identical. Two correction steps are necessary, since the correction procedure with the new points of intersection, based on the same idea as the corrections presented in the one-dimensional case, does not suffice to correct all diffused points. The activation process of nodes in gas or in liquid, with the help of the second correction step (detailed after), is not satisfactory for an accurate computation. Consider, for example, an interface that moves following a diagonal to the mesh, as shown in Fig. 16.

In Fig. 16, during the movement of the interface, some nodes of the mesh initially in gas are reached by the interface and must consequently be activated in liquid. The correction procedure presented in the one-dimensional case, and extended to the two-dimensional case, corrects nodes marked by a circle from state variables of new points of intersection k, $k + 1$, and $k + 2$, in the x and y directions. Nevertheless, this procedure does not allow correction of the node represented by a square in a circle because it is not situated on the same lines i and j for points of intersection. So, these particular nodes must be activated in a gas or liquid by another correction step. In addition to the activation process, this supplementary correction step takes into account the correction of nodes altered by numerical diffusion. Thus, diffused nodes are corrected by two correction steps. Combination

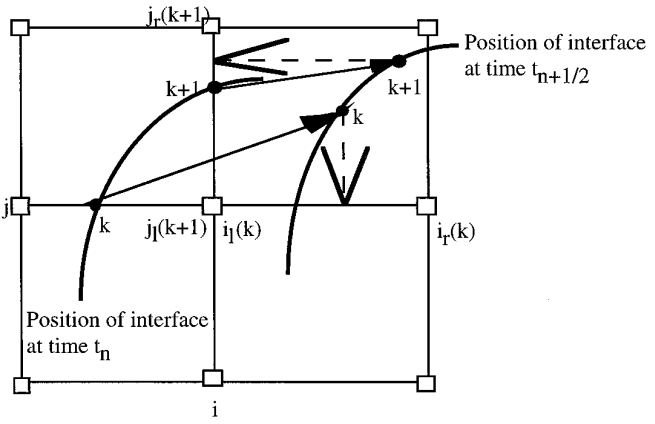

FIG. 17. Correction with projections.

of the two correction procedures ensures an exhaustive correction of all erroneous nodes. We present now these two correction steps.

First correction step. At instant t_n, we know the points of intersection and the states l^* and r^* on both sides of the interface. The movement of points of intersection k and $k + 1$ is calculated from relationship (19). Contrary to the one-dimensional case, these two points are not propagated along mesh lines, as shown in Fig. 17. For the first correction procedure we want to use one-dimensional corrections. The first step of the alternative direction splitting starts at instant t_n and gives solution at instant $t_{n+1/2}$. The first correction procedure uses points of intersection defined at t_n, moved during the time step from t_n to $t_{n+1/2}$ and projected on the x and y axes. States on both sides of the respective projected point, are associated with their projection. So, erroneous nodes can be corrected from linear interpolations, as described in the one-dimensional case. Projection of point k plays the same role as the marker in the one-dimensional case.

Corrections following horizontal and vertical lines must be realized in a very precise order. Indeed, following the x-step of the alternative direction splitting, all nodes affected by diffusion are situated on horizontal lines of the mesh. It is consequently necessary to realize first all corrections in the x-direction and next the y-direction. In the opposite case, corrections for the y-direction may use diffused nodes and give the wrong results.

This first correction step is not able to activate in gas or liquid all nodes swept over by the interface. Indeed (referring to Fig. 18), point k', corresponding to the horizontal projection of the point k at time $t_{n+1/2}$, does not permit activating node $i_r(k)$, since $x(k') < x[i_r(k)]$, although this node has been swept over by the interface (see the one-dimensional correction, considering that k' represents the marker). To remedy the incompleteness of the first correction step, we use a second correction procedure. We remember that the crude first correction is used only to make some erroneous nodes not considered by the more accurate second correction procedure.

Second correction step. When the interface is moved, at instant $t_{n+1/2}$, markers are no longer distributed regularly along the interface. It is therefore necessary to

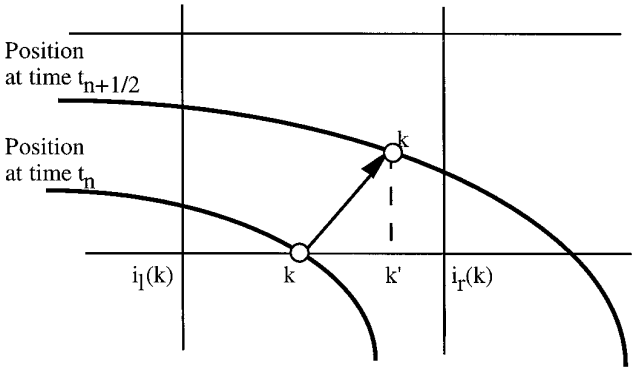

FIG. 18. The nonactivation of node $i_r(k)$.

apply the creation and destruction procedure of markers and thus to reconstruct the interface as described in Gardner *et al.* [13]. When, the interface is correctly reconstructed, it is necessary to seek at instant $t_{n+1/2}$ the new points of intersection between the interface and the mesh lines. The indexes $[i_l(k), i_r(k)]$ or $[j_l(k), j_r(k)]$ relative to each point of intersection k indicate the Eulerian nodes to correct, as shown in Fig. 19. States l^* and r^* of the new points of intersection k, are interpolated from those of markers $i_{cr}(k)$, $i_{cl}(k)$ or $j_{cr}(k)$, $j_{cl}(k)$. We remember that the markers $i_{cr}(k)$, $i_{cl}(k)$ or $j_{cr}(k)$, $j_{cl}(k)$ have been used to create the point of intersection k.

In the correction step, two situations may happen. The first concerns the case where the states of nodes on both sides of a point of intersection correspond to different media. This situation means that the interface remains inside the same cell between instants t_n and $t_{n+1/2}$. One can therefore apply the interpolations, as in the one-dimensional case.

If a point of intersection is situated between two nodes in the same medium, then the interface has moved throughout an adjacent cell and has therefore swept over one of the two nodes. Thus, one of these two nodes must be activated in the

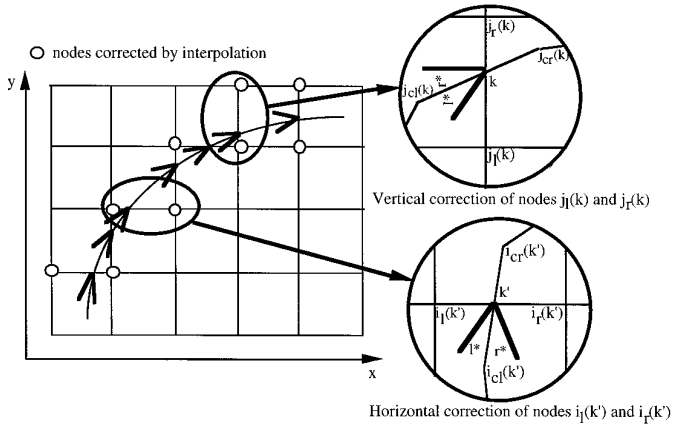

FIG. 19. Eulerian nodes to correct.

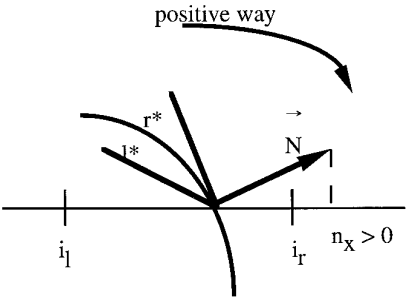

FIG. 20. Activation process of Eulerian points.

liquid or gas, but we do not know what state must be used to activate it. By convention, the normal vector $\vec{N}$ is always oriented from the gaseous phase to the liquid phase. Thus, following the orientation of the normal vector $\vec{N}$, one can identify states l^* and r^* which one must be used for activation. Figure 20 illustrates the procedure for a point of intersection situated on a horizontal line.

If $n_x > 0$, then $U_c^{n+1}(i_r) = U_r^*$, $p_\infty(i_r) = p_{\infty,r}$, $N(i_r) = N_r$ and $U_c^{n+1}(i_l) = U_l^*$, $p_\infty(i_l) = p_{\infty,l}$, $N(i_l) = N_l$. The preceding corrections do not apply, nevertheless, to all topologies of the interface.

Singular topologies. The interface may present some particular topologies during its temporal evolution. In these situations, the proposed correction method must be modified as detailed in the following.

Two points of intersection on both sides of a node. This first particular position concerns the situation where the interface cuts a line of the mesh in two points, on both sides of a node. This particular case is illustrated in Fig. 21. To correct efficiently diffused nodes, it is always necessary to interpolate between the two states corresponding to the same medium and never to interpolate across an interface. Indeed, instead of using $U_E^{n+1}[i_l(k_l) - 1]$ to interpolate $U_C^{n+1}[i_l(k_l)]$ as in the classical correction procedure, we employ $U_{R,r}^{n+1}(k_2)$. The probability of a such situation is weak for interfaces which have a large radius of curvature. However, it becomes more important in the case of several interfaces or when the interface folds over itself.

Two points of intersection in a same cell. This situation corresponds to two points of intersection situated on the same mesh line between two nodes. As shown in

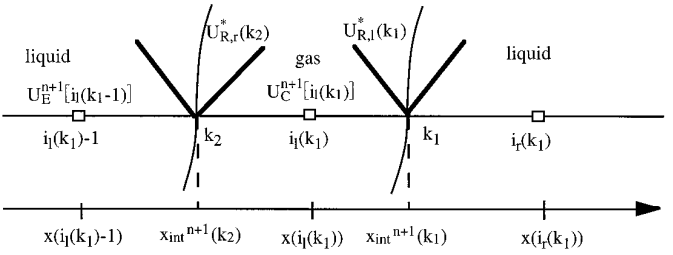

FIG. 21. First singular position of the interface.

FIG. 22. Second singular position of the interface.

Fig. 22, the points of intersection k and k_1 are surrounded by two Eulerian nodes situated in the same medium. In the procedure described previously, the second correction step will activate one of the two nodes in the liquid or gas with the help of states l^* and r^*. So, it is totally wrong to apply this procedure in this situation, since neither of the two points, i_l nor i_r, has been swept over by the interface. So when more than one point of intersection is present between two Eulerian nodes, no correction must be employed. If such a situation occurs physically, the Eulerian mesh must be refined in order to avoid this singular position of interface. But many times, this situation may occur because of roundoff errors when a marker crosses a mesh line on a distance ε ($\varepsilon \approx 0$).

4. RESULTS

Four test cases are presented in order to validate the method. These test cases consider the hydrodynamic behavior of a liquid–gas interface in the presence of shock and rarefaction waves. Despite the imperfections mentioned on the preceding section, we will see that, nevertheless, two-dimensional complex flows can be solved.

4.1. Advection of a Gas Bubble

As we are unable to prove stability and convergence of the algorithm, we choose a simple test case, showing that the interface is stable and well preserved during the calculation. This test case concerns a liquid flow with a gas bubble, having a square shape, situated initially in the left bottom part of the computational domain. The flow moves at uniform velocity. The two phases, liquid and gas, are initially at atmospheric conditions. The computational domain is discretized with a mesh 50×50 and is defined by $0 < x < 1$ m and $0 < y < 1$ m.

In Fig. 23, the liquid–gas interface, given by a succession of markers, is shown at three instants of time $t_1 = 0$ μs, $t_2 = 360$ μs, and $t_3 = 720$ μs. One can observe that the gas bubble is propagated with good accuracy. Nevertheless, the right angles of the bubble are slightly smoothed, since some markers are destroyed or created during reconstruction of the interface. However, as the interface is represented by a large number of markers (about 1100 markers), the angles and shape, as well as the dimensions of the gas bubble, are preserved.

Due to the fact that there is no pressure nor velocity gradient between phases, the flow contains only density and energy discontinuities. We use the density discontinuity to localize the gas bubble in the computational domain. Figure 24 represents the density distribution on the computational domain. Despite the coarse mesh, one can see that the gas–liquid interface is perfectly followed and handled and that

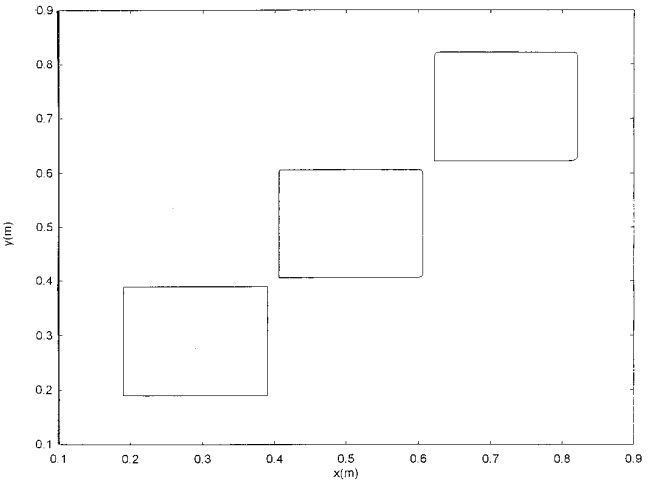

FIG. 23. Position of interface at three instants of time.

no parasitic error disturbs the flow. Furthermore, these results show that mass is well conserved.

4.2. Underwater Explosion

4.2.1. *Square "Bubble"*

As in the one-dimensional case, we consider a simplified model of an underwater explosion that does not take into account the dynamics of the detonation wave and supposes simply that the reaction products are governed by the ideal gas law. One could employ a more realistic equation of state for the detonation products. Solution of the Riemann problem for a real gas law is given in Saurel *et al.* [28], but the introduction of real gas effects would complicate considerably the presentation of the current work. In this configuration, the problem can be considered as a two phase two-dimensional shock tube with a square diaphragm that separates a gas at high pressure and temperature from a liquid at atmospheric conditions. We choose a square diaphragm to appreciate the angle capturing that is usually solved with difficulty. The initial data of the problem are presented in Table II.

Figure 25 shows the exact position of the interface at three instants of time $t_1 = 0\ \mu$s, $t_2 = 45\ \mu$s, and $t_3 = 90\ \mu$s. Initially, the gas bubble possesses a perfectly square shape. After the diaphragm rupture the interface moves throughout the Eulerian mesh, due to the high pressure gradient. During expansion of the gas bubble the interface has a tendency to become circular. However, the angular points of the gas bubble are preserved due to the accurate tracking of the interface. One notes, finally, that the bubble symmetry is perfectly preserved.

Figures 26–27 represent the density distribution over the computational domain at two instants of time, t_2, t_3, and show the two-dimensional evolution of the interface, shock, and rarefaction waves. Indeed, after the diaphragm rupture, a shock wave, followed by the liquid–gas interface, propagates in the liquid while a rarefaction wave moves into the gas.

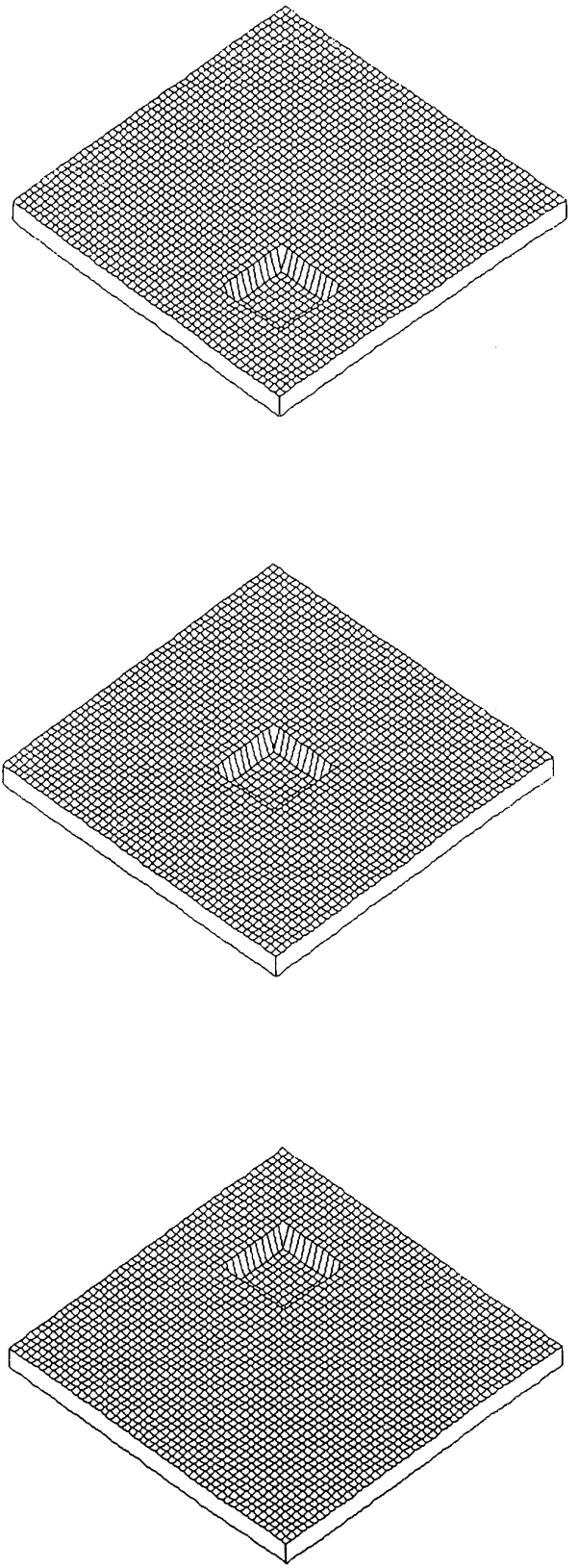

FIG. 24. Density profile at three instants of time.

TABLE II
Initial Data

Initial pressure of detonation products	100,000 atm
Initial temperature of detonation products	3000 K
Initial liquid pressure and temperature	1 atm, 300 K
Initial liquid density	998 kg/m^3
Stiffened Gas EOS parameters for the gas	$N_1 = 1.4$, $p_{\infty,1} = 0$
Stiffened Gas EOS parameters for the liquid	$N_2 = 5.5$, $p_{\infty,2} = 4921.154$

Figure 26, corresponding to instant t_2, shows the strong rarefaction wave that the gas undergoes. These extremely raised values of the density would be greatly decreased if one had employed a real gas equation of state (Saurel *et al.* [28]). One can also notice a weak shock wave that propagates in the liquid. This shock wave is numerically smeared over several cells due to its first-order resolution. The predictor step in our calculations in the 2D code uses the first-order known Godunov scheme. It has been retained for its simplicity, but it produces as is well known, a great smearing of the shock wave. Use of a second-order scheme at the predictor step would reduce its numerical diffusion.

In Fig. 27 one can see that the rarefaction wave reflects at the center of the gas bubble and returns to the interface. Comments concerning the shock and the interface are identical to those of the previous figure. The quality of results is fine, despite first-order resolution of the shock and the rarefaction wave. Otherwise, the symmetry of the problem is well preserved.

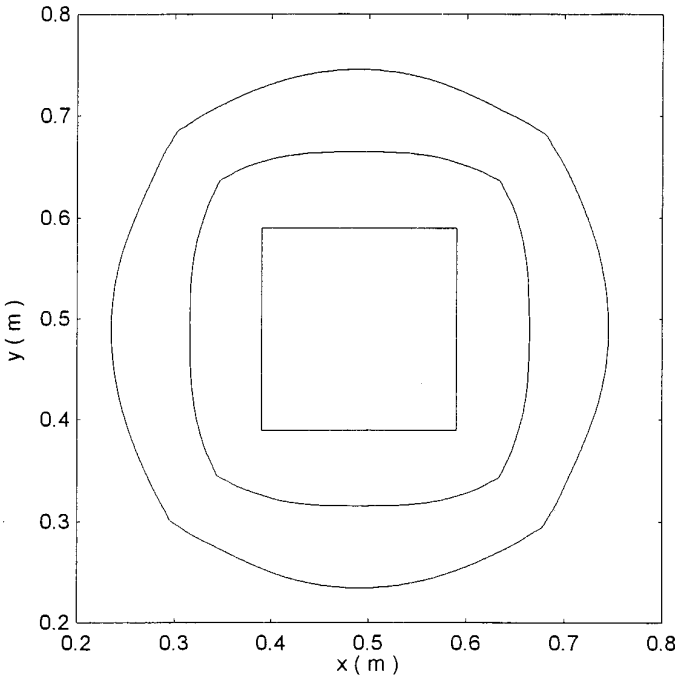

FIG. 25. Position of interface at three instants of time.

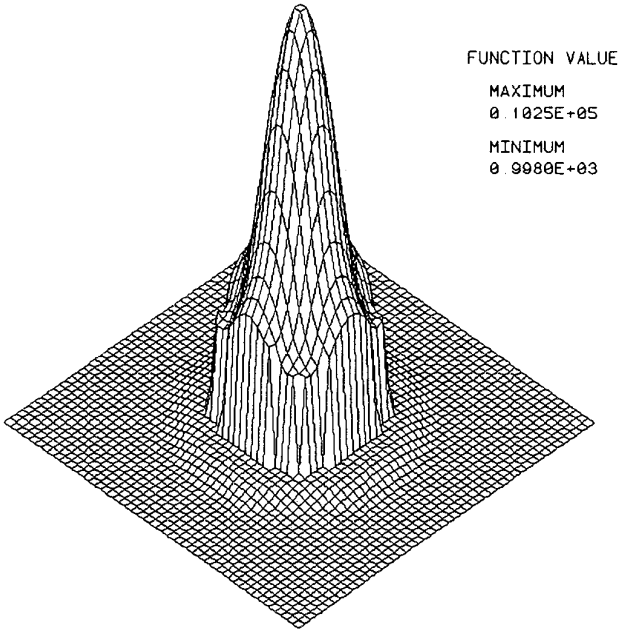

FIG. 26. Density profile at time t_2.

4.2.2. *Circular "Bubble"*

We test the method on a cylindrical "bubble" problem similarly to the last test case. In contrast to the latter, the diaphragm is a circle of radius $r = 0.27$ m and center Ω (0.5, 0.5), and the inital pressure in the gas equals 10,000 atm. Because

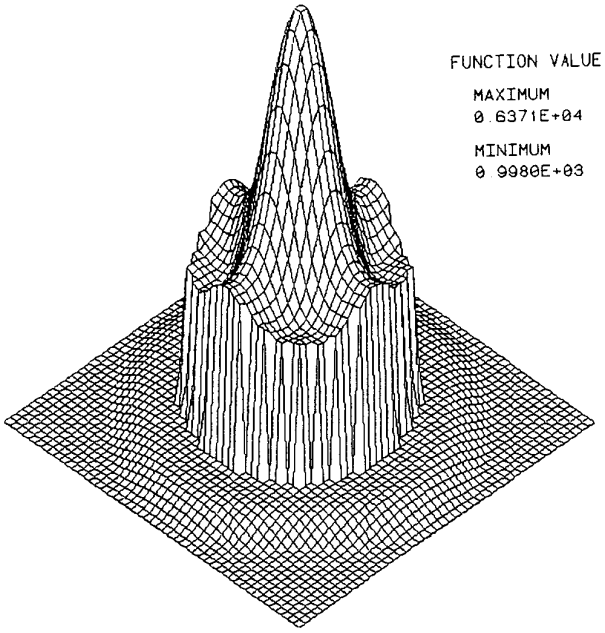

FIG. 27. Density profile at time t_3.

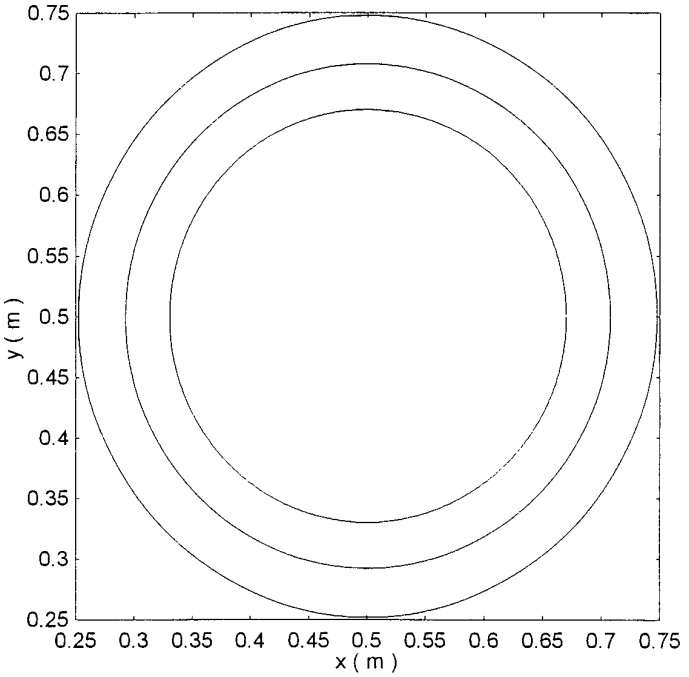

FIG. 28. Position of interface at three instants of time.

of axial symmetry, the two-dimensional problem can be solved with one-dimensional calculations along a radius. So, the one-dimensional solution can be compared with the 2D results.

As seen previously, the one-dimensional calculations were validated by comparing our results with those of Cooke and Chen [6]. So the comparison of one-dimensional and two-dimensional results relative to this kind of underwater explosion validates the two-dimensional calculations.

Similarly to Fig. 25, Fig. 28 shows the positions of the interface at three instants of time, $t_1 = 0$ μs, $t_2 = 60$ μs, and $t_3 = 120$ μs. The shape and the radial symmetry of the interface are perfectly preserved during its temporal evolution. Indeed, the interface is represented by a large number of markers (about 5000 markers) regularly distributed on its cylindrical contour. So it is accurately followed and tracked.

Again, for simplicity reasons the first-order Godunov scheme has been used at the predictor step in both codes. This explains the excessive smearing of the shock waves. Figure 29 represents the density profile at t_2 and t_3, obtained by the 1D and 2D resolutions. The position and the intensity of the shock, interface, and rarefaction waves obtained from these two computations coincide very well. One can consider that the two-dimensional resolution is numerically validated. We now consider a more complex test case.

4.3. Interaction of a Shock Wave with a Cylindrical Gas Bubble

A cylindrical gas bubble of radius $r = 0.27$ m is placed within a liquid. The computational domain is a rectangle of 1 m length and 0.5 m width discretised by the 140×140 mesh. The two media are initially at the same pressure of 100 bar.

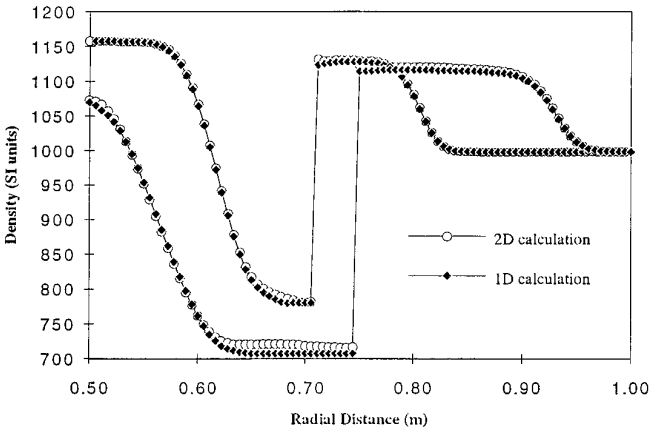

FIG. 29. Comparison between 1D and 2D calculations.

The left side of the studied domain is impacted by a piston at a velocity of 300 m/s. This generates a planar shock wave that propagates in the liquid initially at rest. This shock passes from a medium of high to low acoustic impedance, as illustrated in Fig. 31.

Shock wave interactions with bubbles have been studied experimentally by Hass and Sturtevant [19], Evans [11], and Takayama [30]. Moreover, the propagation of a planar shock over a cylindrical gas bubble has been numerically calculated by Grove and Menikoff [15], using a front tracking method.

Identically to other test cases, Fig. 30 represents the deformation of the interface at several instants. The initial instant $t_1 = 0$ corresponds to a perfectly cylindrical bubble. During the following instant of time, particles of the interface swept over by the shock wave are set into motion while the others remain at rest. During contraction of the bubble the length of the interface decreases and some markers are eliminated. We notice also slight parasitic oscillations of the interface swept over by the shock wave. These oscillations come probably from the approximation

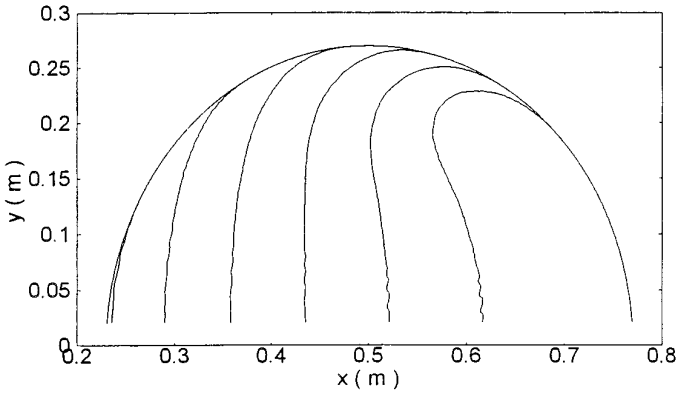

FIG. 30. Position of interface at several instants of time.

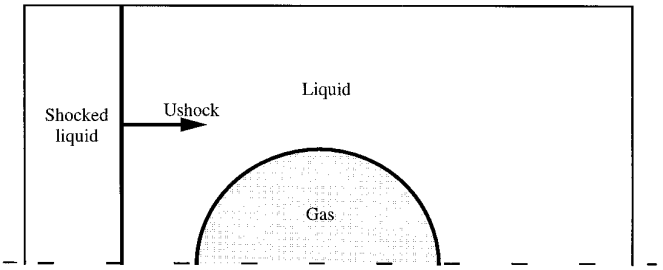

FIG. 31. Interaction of a shock wave with a gas bubble.

made on the determination of the tangential velocity. Despite these slight perturbations, the interface motion seems to be correct. Finally, the last instant corresponds to the situation where the interface begins to fold down over itself. The method treats without difficulty this kind of situation.

When the shock wave hits the gas bubble, this discontinuity diffracts into two waves. Part of the shock wave is transmitted to the gas with a weaker intensity than that of the incident shock. This shock wave propagating into the gas is normal to the interface but is not visible in Figs. 32 and 34 due to the density scale of visualisation. Figure 32 is relative to the density distribution at instant $t_2 = 175\ \mu$s and shows this diffraction of incident shock wave, as shown in Fig. 33.

One observes that the shock velocity in the surrounding liquid is more rapid than that of the shock transmitted into the gas. Two reasons explain this observation. On the one hand, the acoustic impedance of water $(\rho c)_{\text{water}}$ is higher than that of gas $(\rho c)_{\text{gas}}$. On the other hand, the intensity of the shock transmitted to the gas is weaker than that of the water shock. We have therefore a relative movement between phases, or more precisely a sliding of the liquid phase on the gaseous phase. Thus, the tangential velocity is an important parameter in this situation. From the quality of the results, one can confirm that the approximation made on the determination of the tangential velocity is acceptable.

Figure 34 shows the strong bubble contraction at time $t_3 = 350\ \mu$s, when the interface begins to fold down over itself. During the movement of the gas bubble,

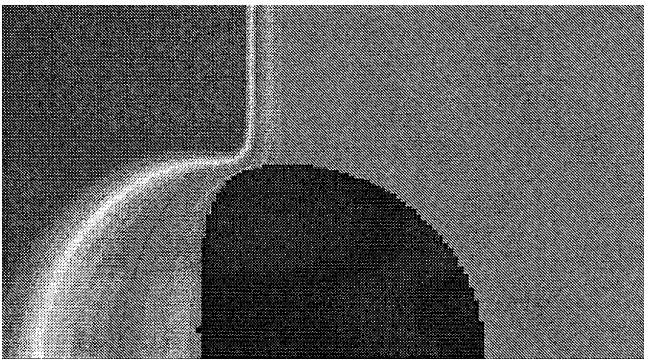

FIG. 32. Density profile at time t_2.

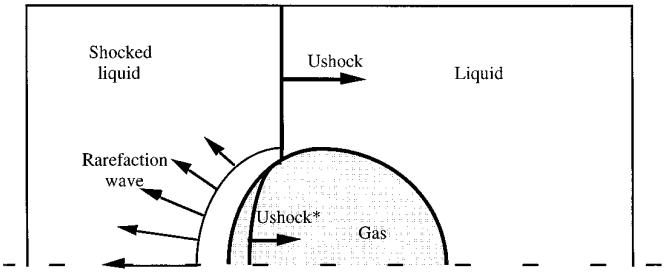

FIG. 33. Diffraction of the initial shock wave.

space liberated by the gas is filled with liquid which collapses behind the bubble, thus creating an overpressure. This overpressure has, as a consequence, to compress the bubble and to move it to the right part of the computational domain.

At the same instant, a rarefaction wave moves backward on the upper part of the liquid around the bubble and disturbs the shock wave that propagates in the liquid as shown in Fig. 34. We have therefore, on the one hand, a compression of the gas bubble and, on the other hand, an expansion of the liquid.

The various phenomena which occur at instant t_3 are illustrated in Fig. 35. A more detailed explanation of these phenomena is given in Grove and Menikoff [15]. A qualitative comparison with the results of this reference shows good agreement between the two simulations.

5. CONCLUSIONS AND PERSPECTIVES

An extension of Godunov-type methods that handles accurately contact discontinuities has been proposed. In the first part, the extension has been developed in one dimension that allows an interface tracking between two compressible media. This new method is based upon the Riemann problem which allows the connection of two media (e.g., liquid and gas) that differ in nature. Solution of the Riemann problem is then inserted into a second order Godunov-type scheme embedded with

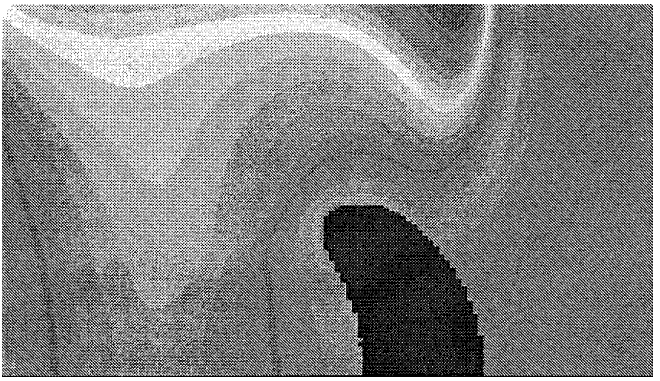

FIG. 34. Density profile at time t_3.

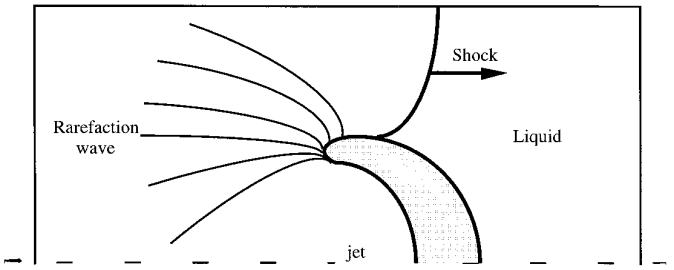

FIG. 35. Main phenomena at time t_3.

the proposed correction procedure. The mixed method allows zero-point capturing of contact discontinuities and good shock capturing. Applied to the one-dimensional case of an underwater explosion, it furnishes good results, in agreement with those of Cooke and Chen [6] and Flores and Holt [12]. A validation of the method is also proposed by comparing the analytical results on the test case of gas–gas and gas–liquid shock tubes. The simplicity of the method renders specific code development easier and no more expensive in terms of computer time than classical Eulerian methods.

In the second part, we have adapted this numerical method in two dimensions. The resolution technique is similar to the one-dimensional method; Euler equations are solved on the overall domain by an Eulerian scheme and nodes situated on both sides of the interface are corrected by interpolations. The system of two-dimensional Euler equations is split into two sets of one-dimensional equations using alternative direction splitting. The interface is represented by a succession of markers regularly distributed along the interface. Velocity and states on both sides of the interface result from the resolution of the exact Riemann problem along the normal to the interface. Contrary to the one-dimensional case, the correction procedure of nodes altered by numerical diffusion consists of two correction steps. First, we use projections of points of intersection defined at the previous time step, while the second uses the new points of intersection of the current time step. The combination of these two steps allows the correction of all nodes situated on both sides of the interface. Furthermore, it ensures the activation of the Eulerian nodes swept over by the interface.

An important restriction of the method is that resolution of the one-dimensional Riemann problem along the normal to the interface does not always approximate well the states on both sides of the interface, especially when the two-dimensional effects within a cell are strong. In all rigor, it would have been necessary to use a two-dimensional exact Riemann solver. Unfortunately, to our knowledge, one does not currently exist.

However, this approximation does not produce large errors for many applications. Despite this restriction, the proposed method allows one to treat accurately many multimaterial and two-dimensional problems. The results for four test cases are given. The first one describes the motion of the gas bubble in a uniform velocity field and shows that interfaces are correctly advected, despite the coarse mesh. The second one concerns a simplified model of an underwater explosion and allows

one to observe the perfect symmetry of the two-dimensional liquid–gas interface. Angular points are also preserved. The third is relative to the cylindrical explosion problem which allows validating the two-dimensional resolution. Finally, the last test case describes the interaction of a shock with a gas bubble. It shows that the method treats correctly the situation where the interface folds down over itself.

The method described in this paper is a front tracking method. Its accuracy has been demonstrated on several test cases. Development of such a method in 1D, is very easy, while its extension to 2D, as developed herein is not so simple. General configurations in 3D with an arbitrary number of materials seems to be very complicated. Effort must be continued to render a simpler multimaterial algorithm in compressible media.

Alternatives to the front tracking method have been proposed very recently in Abgrall [2] and Karni [21]. These methods are full Eulerian and seem to be very efficient and propose new ways for multifluid problems. We are examining these methods too.

ACKNOWLEDGMENTS

This research has been partially supported by CTSN Toulon. Dr. Tosello is gratefully acknowledged.

REFERENCES

1. R. Abgrall, Generalisation of Roe scheme for the computation of mixture of perfect gases, *Rech. Aérosp.* **6,** 31 (1988).
2. R. Abgrall, How to prevent pressure oscillation in multicomponent flow calculation: A quasi conservation approach, *J. Comput. Phys.* **125,** 150 (1996).
3. D. L. Book, J. P. Boris, and K. Haim, Flux corrected transport II: Generalisation of the method, *J. Comput. Phys.* **18,** 243 (1975).
4. I. L. Chern, J. Glimm, O. McBryan, B. Plohr, and S. Yaniv, Front tracking for gas dynamics, *J. Comput. Phys.* **62,** 83 (1985).
5. P. Collela and H. M. Glaz, Efficient solution algorithm for the Riemann problem for the real gases, *J. Comput. Phys.* **59,** 264, (1985).
6. C. H. Cooke and T. J. Chen, Continuous front tracking with subcell resolution, *J. Sci. Comput.* **6,** 269 (1991).
7. A. J. Chorin, Random choice solution of hyperbolic systems, *J. Comput. Phys.* **22,** 517 (1976).
8. D.-K. Mao, A treatment of discontinuities for finite difference methods in the two-dimensional case, *J. Comput. Phys.* **104,** 377 (1993).
9. D.-K. Mao, A treatment of discontinuities for finite difference methods, *J. Comput. Phys.* **103,** 359 (1992).
10. D.-K. Mao, A treatment of discontinuities in shock-capturing finite difference methods, *J. Comput. Phys.* **92,** 422 (1991).
11. M. W. Evans, Intersection of shock or rarefaction with a bubble, *Phys. Fluids,* **5,** 651 (1962).
12. J. Flores and M. Holt, Glimm's method applied to underwater explosions, *J. Comput. Phys.* **44,** 377 (1981).
13. C. L. Gardner, J. Glimm, O. McBryan, R. Menikoff, D. H. Sharp and Q. Zhang, The dynamics of bubble growth for Rayleigh–Taylor unstable interface, *Phys. Fluids* **31,** 447 (1988).
14. S. K. Godunov, A difference method for numerical calculation of discontinuous solutions of hydrodynamics, *Mat. Sb.* **47,** 271 (1959).

15. J. Grove and R. Menikoff, The anomalous reflection of a shock wave at a material interface, *J. Fluid. Mech.* **219,** 313 (1990).
16. J. Glimm, Solutions in the large for nonlinear hyperbolic systems of equations, *Comm. Pure Appl. Math.* **18,** 697 (1965).
17. F. Harlow and A. Amsden, *Fluid dynamics*, LANL Monograph LA-4700, 1971.
18. A. Harten, ENO schemes with subcell resolution, *J. Comput. Phys.* **83,** 148 (1988).
19. J.-F. Hass and B. Sturtevant, Interaction of weak shock with cylindrical and spherical gas inhomogeneities, *J. Fluid. Mech.* **181,** 41 (1987).
20. S. Karni, Multicomponent flow calculations by a consistent primitive algorithm, *J. Comput. Phys.* **112,** 31 (1994).
21. S. Karni, Hybrid multifluid algorithms, *SIAM J. Comput.* **17,** 1019 (1996).
22. R. J. LeVeque and K.-M. Shyue, One dimensional front tracking based on high resolution wave propagation methods, *SIAM J. Sci. Comput.* **16,** 348 (1995).
23. R. Menikoff and B. Plohr, The Riemann problem for fluid flow of real materials, *Rev. Mod. Phys.* **61,** 75 (1989).
24. W. Mulder, S. Osher, and J. A. Sethian, Computing interface motion in compressible gas dynamics, *J. Comput. Phys.* **100,** 209 (1992).
25. S. Osher, Convergence of generalized MUSCL schemes, *SIAM J. Numer. Anal.* **21,** 360 (1985).
26. B. J. Plohr, Shockless acceleration of thin plates modeled by a tracking random choice method, *AIAA J.* **26,** 470 (1988).
27. P. L. Roe, Approximate Riemann solvers, parameter vectors and difference schemes, *J. Comput. Phys.* **43,** 357 (1981).
28. R. Saurel, M. Larini, and J.-C. Loraud, Exact and approximate Riemann solvers for real gases, *J. Comput. Phys.* **112,** 126 (1994).
29. G. Strang, On the construction and comparison of difference schemes, *SIAM J. Numer. Anal.* **5,** 506 (1968).
30. K. Takayama, Holographic interferometric study of shock wave propagation in two-phase media, in *Shock Tubes and Waves, Proc. 16th Intl. Symp. on Tubes and Waves, Aachen, 51–62, 1987*, edited by H. Grönig.
31. E. F. Toro, *Riemann Solvers and Upwind Methods for Fluid Dynamics* (Springer-Verlag, New York/Berlin, 1997).
32. B. Van Leer, Toward the ultimate conservative difference scheme. A second order sequel to Godunov's method, *J. Comput. Phys.* **32,** 101 (1979).
33. J. Von Neumann and R. D. Richtmyer, A method for the numerical calculations of hydrodynamic shocks, *J. Appl. Phys.* **21,** 232 (1950).